LETTERS

Structure and mechanism of the M2 proton channel of influenza A virus

Jason R. Schnell[1] & James J. Chou[1]

The integral membrane protein M2 of influenza virus forms pH-gated proton channels in the viral lipid envelope[1]. The low pH of an endosome activates the M2 channel before haemagglutinin-mediated fusion. Conductance of protons acidifies the viral interior and thereby facilitates dissociation of the matrix protein from the viral nucleoproteins—a required process for unpacking of the viral genome[2]. In addition to its role in release of viral nucleoproteins, M2 in the trans-Golgi network (TGN) membrane prevents premature conformational rearrangement of newly synthesized haemagglutinin during transport to the cell surface by equilibrating the pH of the TGN with that of the host cell cytoplasm[3]. Inhibiting the proton conductance of M2 using the anti-viral drug amantadine or rimantadine inhibits viral replication[4–7]. Here we present the structure of the tetrameric M2 channel in complex with rimantadine, determined by NMR. In the closed state, four tightly packed transmembrane helices define a narrow channel, in which a 'tryptophan gate' is locked by intermolecular interactions with aspartic acid. A carboxy-terminal, amphipathic helix oriented nearly perpendicular to the transmembrane helix forms an inward-facing base. Lowering the pH destabilizes the transmembrane helical packing and unlocks the gate, admitting water to conduct protons, whereas the C-terminal base remains intact, preventing dissociation of the tetramer. Rimantadine binds at four equivalent sites near the gate on the lipid-facing side of the channel and stabilizes the closed conformation of the pore. Drug-resistance mutations are predicted to counter the effect of drug binding by either increasing the hydrophilicity of the pore or weakening helix–helix packing, thus facilitating channel opening.

M2 is a 97-residue single-pass membrane protein that has its amino and carboxy termini directed towards the outside and inside of the virion, respectively; it is a homotetramer in its native state[8,9]. The four transmembrane helices form a channel in which His 37 is the pH sensor and Trp 41 is the gate[6,10,11]. The adamantane-based drugs amantadine and rimantadine, which target the M2 channel, have been used as first-choice antiviral drugs against community outbreaks of influenza A viruses for many years, but resistance to the adamantanes has recently become widespread. Many structural models of this channel have been built, based on sequence analysis, mutagenesis and solid-state NMR[8,11,12]. Many of these studies have been done on inherently unstable transmembrane-only constructs, however, leading to conflicting structural conclusions.

Although the transmembrane-only peptide fails to form a stable tetramer, a construct of residues 18–60 (M2(18–60)), which includes 15 residues of the C terminus in addition to the transmembrane region, forms a stable tetramer in dihexanoyl-phosphatidyl-choline (DHPC) detergent micelles and yields high-resolution NMR spectra (Supplementary Fig. 1). In the closed conformation at pH 7.5, M2(18–60) is a homotetramer in which each subunit has an unstructured N terminus (residues 18–23), a channel-forming transmembrane helix (residues 25–46), a short flexible loop (residues 47–50) and a C-terminal amphipathic helix (residues 51– 59). The transmembrane helices assemble into a four-helix bundle with a left-handed twist angle of ~23° and a well defined pore (Fig. 1). A ring of methyl groups from Val 27 constricts the N-terminal end of the pore to ~3.1 Å (inner diameter). In agreement with proposed models[11,13], His 37 and Trp 41 are inside the pore. A three-bond, ^{15}N–$^{13}C\gamma$ scalar coupling ($^{3}J_{NC\gamma}$) value of 1.5 Hz (Supplementary Table 1) shows the His 37 χ_1 rotamer to be predominantly *trans*, but with significant rotameric averaging. The χ_1 of Trp 41 is essentially locked in the *trans* position, as determined by a $^{3}J_{NC\gamma}$ of 2.6 Hz, whereas the χ_2 is also fixed at around −120° by the side chain Hε1–Nε1 dipolar coupling and nuclear Overhauser effects (NOEs). The Trp 41 indole rings are at van der Waals distance from each other, prohibiting passage of water or ions (Fig. 1c). The indole Hε1 of one subunit is on average 3.5 Å from the Asp 44 carboxyl carbon of the adjacent subunit. The two residues can form an intermolecular hydrogen bond that stabilizes the closed Trp 41 gate. The side chain of Arg 45 probably participates in an intermolecular interaction with Asp 44. These findings are consistent with the increased pH-modulated activity of channels in which asparagine has replaced Asp 44 (ref. 14).

The C-terminal end of the channel extends into a loop (residues 47–50) that connects the transmembrane domain to the C-terminal amphipathic helix. Residual dipolar couplings (RDCs) and intra- and inter-monomer NOEs show that the amphipathic helices lie roughly perpendicular (~82°) to the transmembrane helices and assemble head-to-tail using a right-handed packing mode to form the base of the channel. The orientation and amphipathic character of the amphipathic helices suggest that the C-terminal base lies on the surface of the membrane.

Residues 47–50 give no NOE peaks and do not have a stable, hydrogen-bonded structure in the detergent micelles used in our work. We believe that this segment adopts a more stable conformation in the viral membrane because Cys 50, which we mutated to serine to avoid disulphide formation, is normally palmitoylated[15]. Modelling shows that extending the transmembrane helix to Phe 48 would place residue 50 facing the membrane, allowing for insertion of the palmitoyl acyl chain into the lipid bilayer. This minor rearrangement would also move the amphipathic helices closer to the transmembrane domain.

Drug binding stabilizes the closed conformation. On addition of drug, the resonances of residues 43–46 at the C terminus of the channel, which are severely exchange-broadened in the drug-free sample, became significantly sharper and more homogeneous (Supplementary Fig. 2). The protein–drug NOEs collected from four different NOE spectroscopy (NOESY) spectra (Supplementary Fig. 3) place the binding site between adjacent helices at the C-terminal end of the transmembrane domain near the Trp 41 gate, on the membrane side of the channel (Fig. 1d). We could not detect

[1]Department of Biological Chemistry and Molecular Pharmacology, Harvard Medical School, Boston, Massachusetts 02115, USA.

drug NOEs in other parts of the protein, including the widely proposed drug-binding site in the pore of the channel. The amine headgroup of rimantadine is in contact with the polar side chains of Asp 44 and Arg 45, and with the indole amine of Trp 41. The side chains of Ile 42 from one helix and Leu 40 and Leu 43 from another helix form the hydrophobic walls of the binding pocket that interact with the adamantane group of rimantadine. Thus, rimantadine covers a unique polar patch in the otherwise hydrophobic environment of the transmembrane domain. Interactions between rimantadine and the channel are consistent with structure–activity relationships of the adamantane group[16]. In particular, the basic nitrogen group and size limits at the methyl site are critical. These requirements are the result of the interactions with Asp 44 and the small hydrophobic pocket around Ile 42, respectively.

Water NOEs measured in the 110-ms ^{15}N-separated NOESY experiments give a clear picture of water distribution relative to the channel (Fig. 2). The lipid-facing surface of the transmembrane region is largely protected from water by the DHPC micelle. In the closed channel pore, the Val 27 ring at the N terminus and the Trp 41 gate at the C terminus essentially block water from freely diffusing into the pore from either side of the membrane. Within the transmembrane region, only the amides of Ser 31 and Ile 32 have NOE crosspeaks at the chemical shift of water, probably corresponding to the hydroxyl proton of Ser 31 in exchange with water. A polar residue is present at position 31 in all sequenced variants of M2, suggesting that proton conduction requires water to be bound to this site. This water may serve to bridge the proton relay from the N-terminal end of the pore to the His 37 pH sensor. Water was detected at the C terminus of the transmembrane region, beginning at Arg 45. The Hε1 of the Trp 41 indole ring, which points towards the C-terminal side of the pore, also has a strong NOE to water, indicating that the base of the channel is accessible to bulk water.

Lowering the pH from 7.5 to 6.5 broadens most of the NMR resonances corresponding to the transmembrane helix (Fig. 3a). The resonance broadening could not be attributed to protein aggregation, because the self-diffusion coefficients were essentially unchanged between pH 7.5 and pH 6.5. Thus, activation of the channel is coupled to increased conformational exchange in the transmembrane domain. In contrast, the resonances of the amphipathic helices are essentially unaffected by lowering the pH, indicating that the C-terminal base of the tetramer remains intact as the channel opens.

In addition to destabilizing helix–helix packing in the transmembrane domain, channel activation must also correlate with increased dynamics of the Trp 41 gate. Because the indole amide resonance of Trp 41 remained strong as the pH was lowered from 7.5 to 6.0, it serves as a useful NMR probe for monitoring opening of the channel. We compared the millisecond timescale dynamics of the Trp 41 indole ring between the closed and open states by carrying out relaxation-compensated Carr–Purcell–Meiboom–Gill (CPMG) experiments[17] at pH 7.5, pH 7.0 and pH 6.0. A two-site exchange model fits the dependence of ^{15}N relaxation caused by chemical shift exchange on the frequency of refocusing ($1/\tau_{cp}$) of chemical shift evolution (Fig. 3b), implying that the gate switches between two configurations at any given pH. As the pH was lowered from 7.5 to 6.0, the rate of fluctuation increased by more than fourfold (Fig. 3b), indicating that channel activation 'unlocks' the gate. Adding rimantadine to the channel at an intermediate pH of 7.0 slowed the timescale of the gate motion to nearly that of a drug-free gate at pH 7.5 (Fig. 3c). These results confirm that the reconstituted channels in the

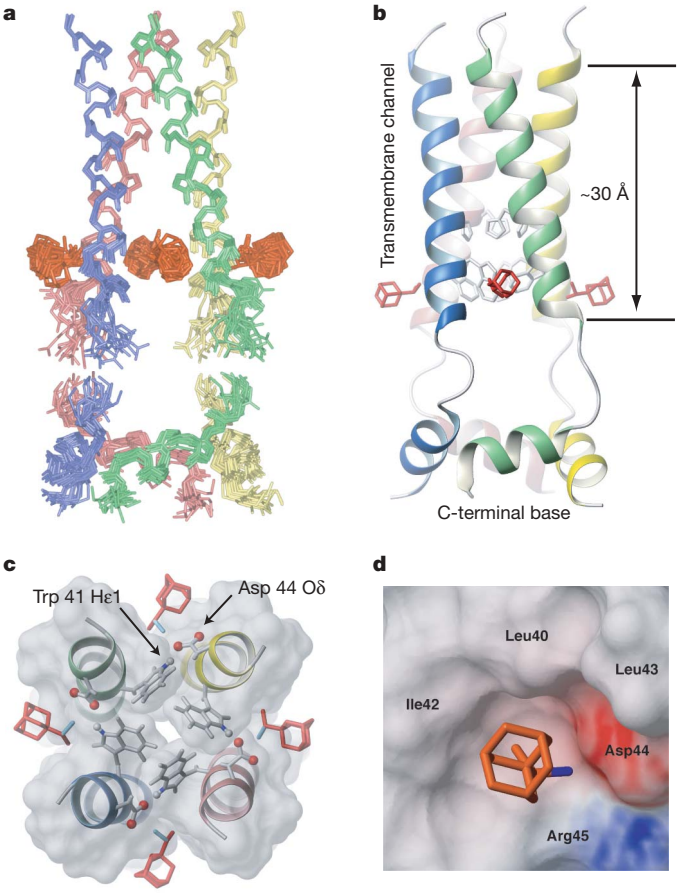

Figure 1 | Structure of the M2 channel. **a**, An ensemble of 15 low-energy structures derived from NMR restraints. Because residues 47–50 are unstructured, the transmembrane helices (residues 25–46) and the amphipathic helices (residues 51–59) are superimposed separately. The backbone r.m.s. deviations for the transmembrane and amphipathic helices are 0.30 Å and 0.56 Å, respectively. **b**, A ribbon representation of a typical structure from the ensemble in **a**, showing the left-handed packing of the transmembrane helices, right-handed packing of the amphipathic helices, the side chains of His 37 and Trp 41, and the drug rimantadine (coloured in red). **c**, A close-up view from the C-terminal side of the channel showing the Trp 41 gate and how it is stabilized by the inter-monomer hydrogen bond between Trp 41 Hε1 of one transmembrane helix and Asp 44 carboxyl of the adjacent transmembrane helix. **d**, The surface representation of the rimantadine-binding pocket, showing the Asp 44, the indole amine of Trp 41, and Arg 45, which form the polar patch, as well as the hydrophobic wall composed of Leu 40, Ile 42 and Leu 43.

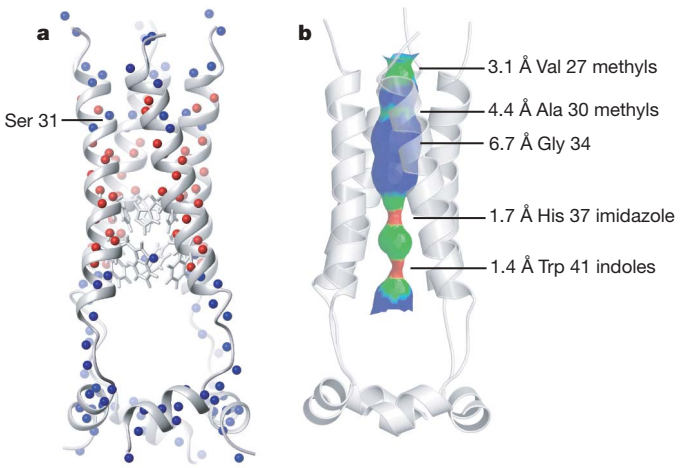

Figure 2 | Water accessibility of the M2 channel. **a**, Distribution of water NOEs relative to the structure. Amide protons coloured in blue have a NOE crosspeak to water. Those that do not are coloured red. **b**, The pore surface calculated using the program HOLE. The region of the channel coloured in green is only wide enough to allow passage of a water molecule, whereas the blue portion can accommodate two or more water molecules. The orange region is too narrow to allow any ions to pass through.

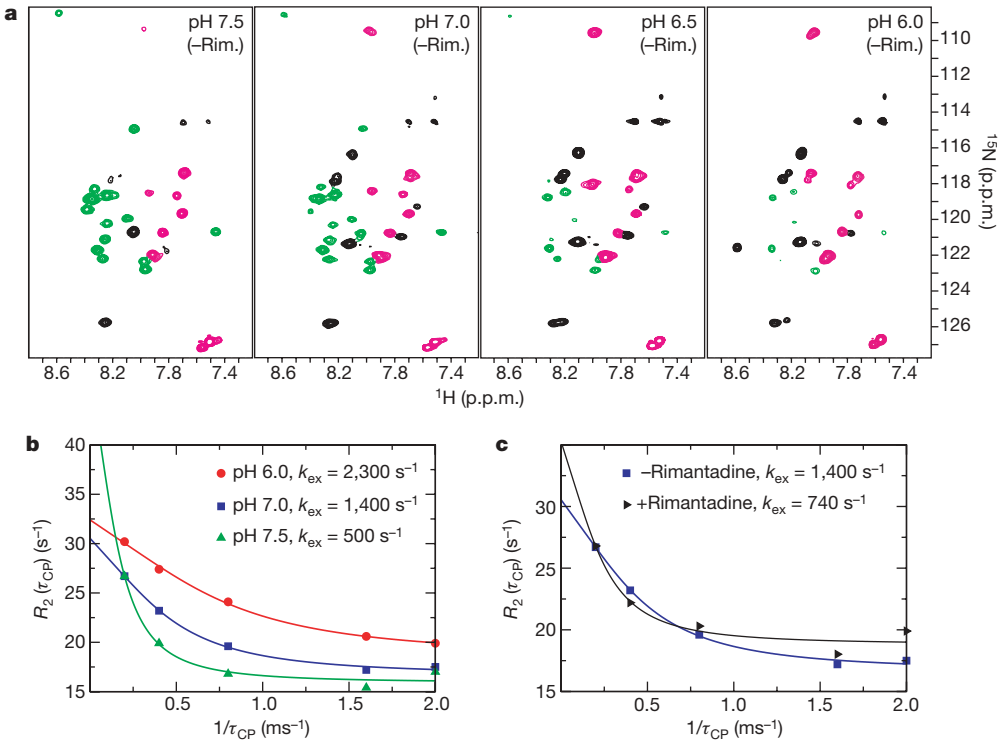

Figure 3 | Low-pH-induced destabilization of the channel and opening of the Trp 41 gate. **a**, ^{1}H-^{15}N TROSY spectra of reconstituted M2(18–60) tetramer at pH 6.0, 6.5, 7.0 and 7.5, in the absence of rimantadine (−Rim.), recorded at 500 MHz ^{1}H frequency and 30 °C. Green, transmembrane helix; pink, amphipathic helix; black, N-terminal loop. **b**, The ^{15}N R_2 (pure $R_2 + R_{ex}$) of the Trp 41 Nε1 as a function of the frequency of refocusing (1/τ_{cp}) of chemical shift evolution obtained at pH 7.5, 7.0 and 6.0, showing faster timescale motion of the Trp 41 gate as the channel is activated. **c**, Comparison between $R_2(\tau_{cp})$ at pH 7.0 in the absence (blue) and presence (black) of rimantadine, demonstrating that the drug slows down the gate flipping at this pH.

NMR sample are pH-gated, and are consistent with the location of the rimantadine site proximal to the gate.

The structure of the M2 proton channel thus reveals a simple yet effective gating. The tight packing of the four transmembrane helices brings the bulky indole rings of Trp 41 into van der Waals contact to form the channel gate. The gate is further stabilized by inter-subunit hydrogen bonds with Asp 44. Lowering the pH protonates the imidazole rings of His 37, destabilizing helix–helix packing by electrostatic repulsion. This conformational rearrangement breaks interactions between Trp 41 and Asp 44 and allows the gate to flip open. A pair of conserved N-terminal cysteines have been shown to form intermolecular disulphides *in vivo*[9]. Thus, the transmembrane helices are tethered at one end by N-terminal disulphides and at the other end by the C-terminal base, ensuring that destabilization of the four-helix bundle during channel activation does not cause dissociation of the tetramer (Fig. 4). Indeed, truncation of the amphipathic helix results in channels that rapidly lose channel activity[18].

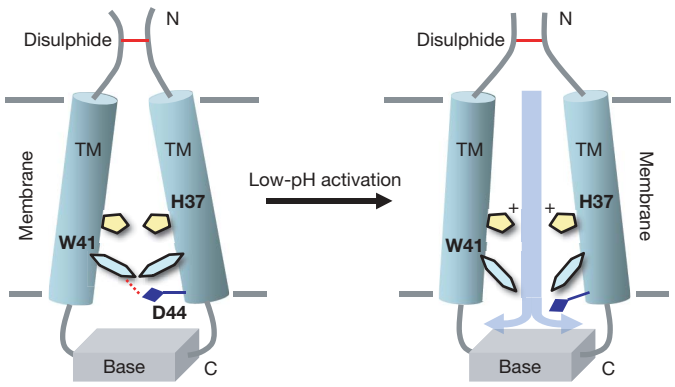

Figure 4 | Schematic illustration of M2 channel activation. At high pH, the transmembrane (TM) helices are packed tightly and the tryptophan gate is locked through intermolecular interactions with Asp 44. At low pH, protonation of the His 37 imidazoles destabilizes the transmembrane helix packing, allowing hydration of the channel pore and proton conductance. The C-terminal base of the tetramer and N-terminal disulphide bonds keep the channel from completely disassembling. For clarity, only two of the four monomers are shown.

The discovery of the external drug-binding site was unexpected. Drug-resistance mutations seemed to suggest that the drug-binding site was inside the pore, because, in early models of the channel, residues that lead to drug resistance were predicted to be pore-lining. The known mutations that confer drug resistance are L26F, V27A, A30T, S31N, G34E and L38F. Mapping these residues onto the structure (Supplementary Fig. 7) reveals that Val 27, Ala 30 and Gly 34 are pore-lining, but that Leu 26, Ser 31 and Leu 38 are in the helix–helix packing interface. Moreover, these mutations are spread out over more than three turns of the transmembrane helix, covering a distance much larger than the dimensions of amantadine or rimantadine. The authors of ref. 19 pointed out that having a cork-plugging-the-bottle model is insufficient to explain all the results of electrophysiology studies. For example, drug inhibition is more effective when applied to the closed channel than to the open channel, which is not expected of a pore-blocking mechanism[5]. Several of the drug-resistance mutations in pore-lining residues have been shown to retain drug binding[20]. Although a pore blocker is expected to fit tightly in the pore, channel inhibition is unusually tolerant of modifications to the adamantane scaffold[16]. Together, the above observations suggest an allosteric inhibition mechanism.

Is the external binding site consistent with all drug-resistance mutations? Although the exact structural effects of resistance mutations are difficult to predict, what they do have in common is that they either perturb the helix–helix interface (L26F, V27A, S31N, L38F) or increase the hydrophilicity of the pore (A30T, G34E).

From this observation, and from detection of a conformational exchange among multiple states at lowered pH, we propose an allosteric inhibition mechanism that can account for all of the mutations. In our model, drug binding makes the closed channel harder to open, whereas drug-resistance mutations destabilize the closed channel, making it easier to open. Replacing Val 27 with alanine enlarges the N-terminal opening and weakens helix–helix packing, and therefore may facilitate channel opening. Ala 30 and Gly 34 are inside the pore, and replacing them with threonine and glutamate, respectively, may facilitate pore hydration, and, in turn, channel opening. Leu 26, Ser 31 and Leu 38 are helix–helix interface residues; their mutations probably perturb helix–helix packing and lower the energetic cost of channel opening.

Why, then, are no drug-resistant mutations observed near the drug-binding site? In fact, few mutations are ever observed in this region of the channel (drug-resistant or otherwise), which is not surprising owing to the functional constraints placed on these residues in proximity to the channel pH sensor (His 37) and the channel gate (Trp 41). As the structure illustrates, intermolecular contacts between Asp 44 and Arg 45 form an integral part of the channel gate, along with Trp 41. The residues that form the hydrophobic walls of the binding pocket—Leu 40, Ile 42 and Leu 43—are on the lipid face of the channel and must retain hydrophobicity for membrane partitioning. To accommodate the Trp 41 indole rings within the channel, the helices splay slightly at the C terminus of the transmembrane domain, and interhelical contacts below Leu 38—with the exception of the Trp 41 side chains—are no longer important for channel assembly. Thus, residues essential to channel assembly are in the N-terminal half of the transmembrane helix, exactly where drug-resistance mutations occur.

Binding from the membrane side is consistent with the high membrane partition coefficient of adamantane drugs, which effectively concentrates them in the membrane and lowers their level in the aqueous phase[21,22]. Adamantanes interact with a number of other ion channels, including viroporins from hepatitis C[23], the potassium channel Kcv of the chlorella virus PBCV-1 (ref. 24) and the human NMDA receptors[25]. Hanatoxin, an allosteric inhibitor of voltage-gated K^+ channels with a high membrane partition coefficient, also has an external binding site[26,27]. Membrane-side binding may thus be a feature of many channel inhibitors. This mode of inhibition could be advantageous for drug design because drug molecules are typically much larger than hydrated ions selected by ion channels, and therefore the energy barrier for the drug to find a blocking site inside the channel pores would be much higher than targeting a functional site from the membrane side of the channel.

Note added in proof: We note that, in a separate X-ray study of the transmembrane domain of M2, an electron density, which was proposed to be from amantadine, was observed inside the channel pore (see ref. 28).

METHODS SUMMARY

The M2(18–60) polypeptide construct was expressed as a C-terminal fusion to bacterial trpLE with an N-terminal His_9 tag in the pMM-LR6 vector[29]. The M2(18–60) tetramer was reconstituted by dissolving peptide in a solution containing 50 mM sodium phosphate, 6 M guanidine HCl and 150 mM DHPC, dialyzing against a solution containing 40 mM sodium phosphate (pH 7.5) and 30 mM glutamate, and concentrating. Rimantadine was added to the reconstituted protein. The final NMR sample used for structure determination contained 0.75 mM M2(18–60) (monomer), ~300 mM DHPC and 40 mM rimantadine. Given that the DHPC has an aggregation number of 27 (ref. 30) and the strong partition coefficient of rimantadine in phospholipids (rimantadine aqueous solubility is very low, ~50 μM), locally, there are about four rimantadine molecules per micelle compartment in which the channel resides.

The NMR protocol used was similar to that described previously[31]. An extensive set of structural restraints (including 230×4 intra- and 27×4 inter-molecular distance restraints derived from NOEs, 27×4 orientation restraints from residual dipolar couplings (RDCs), and 23×4 side-chain rotamers from three-bond scalar couplings) were used to generate an ensemble of 15 low-energy structures with a backbone root mean square (r.m.s.) deviation of 0.30 Å for the channel region and of 0.89 Å for all structured regions (Fig. 1a). The refinement statistics and NMR-derived restraints are summarized in Supplementary Table 1. Structure calculation was accomplished in two steps, in which the overall tetramer conformation was first defined by NOE-derived distance restraints and *J*-coupling-derived dihedral restraints using a high-temperature simulated annealing protocol, and was subsequently refined against RDCs at low temperature.

Full Methods and any associated references are available in the online version of the paper at www.nature.com/nature.

Received 15 July; accepted 3 December 2007.

1. Lamb, R. A., Holsinger, L. J. & Pinto, L. H. *Receptor-Mediated Virus Entry into Cells* (ed., Wimmer, E.) 303–321 (Cold Spring Harbor Laboratory Press, Cold Spring Harbor, 1994).
2. Helenius, A. Unpacking the incoming influenza-virus. *Cell* **69,** 577–578 (1992).
3. Ciampor, F. *et al.* Evidence that the amantadine-induced, M2-mediated conversion of influenza A virus hemagglutinin to the low pH conformation occurs in an acidic trans Golgi compartment. *Virology* **188,** 14–24 (1992).
4. Hay, A. J., Wolstenholme, A. J., Skehel, J. J. & Smith, M. H. The molecular basis of the specific anti-influenza action of amantadine. *EMBO J.* **4,** 3021–3024 (1985).
5. Wang, C., Takeuchi, K., Pinto, L. H. & Lamb, R. A. Ion channel activity of influenza A virus M2 protein: characterization of the amantadine block. *J. Virol.* **67,** 5585–5594 (1993).
6. Pinto, L. H., Holsinger, L. J. & Lamb, R. A. Influenza virus M2 protein has ion channel activity. *Cell* **69,** 517–528 (1992).
7. Chizhmakov, I. V. *et al.* Selective proton permeability and pH regulation of the influenza virus M2 channel expressed in mouse erythroleukaemia cells. *J. Physiol. (Lond.)* **494,** 329–336 (1996).
8. Sugrue, R. J. & Hay, A. J. Structural characteristics of the M2 protein of influenza A viruses: evidence that it forms a tetrameric channel. *Virology* **180,** 617–624 (1991).
9. Holsinger, L. J. & Lamb, R. A. Influenza virus M2 integral membrane protein is a homotetramer Stabilized by formation of disulfide bonds. *Virology* **183,** 32–43 (1991).
10. Tang, Y., Zaitseva, F., Lamb, R. A. & Pinto, L. H. The gate of the influenza virus M2 proton channel is formed by a single tryptophan residue. *J. Biol. Chem.* **277,** 39880–39886 (2002).
11. Pinto, L. H. *et al.* A functionally defined model for the M2 proton channel of influenza A virus suggests a mechanism for its ion selectivity. *Proc. Natl Acad. Sci. USA* **94,** 11301–11306 (1997).
12. Wang, J. F., Kim, S., Kovacs, F. & Cross, T. A. Structure of the transmembrane region of the M2 protein H^+ channel. *Protein Sci.* **10,** 2241–2250 (2001).
13. Kukol, A., Adams, P. D., Rice, L. M., Brunger, A. T. & Arkin, I. T. Experimentally based orientational refinement of membrane protein models: A structure for the influenza A M2 H^+ channel. *J. Mol. Biol.* **286,** 951–962 (1999).
14. Betakova, T., Ciampor, F. & Hay, A. J. Influence of residue 44 on the activity of the M2 proton channel of influenza A virus. *J. Gen. Virol.* **86,** 181–184 (2005).
15. Sugrue, R. J., Belshe, R. B. & Hay, A. J. Palmitoylation of the influenza A virus M2 protein. *Virology* **179,** 51–56 (1990).
16. Aldrich, P. E. *et al.* Antiviral agents. 2. Structure–activity relationships of compounds related to 1-adamantanamine. *J. Med. Chem.* **14,** 535–543 (1971).
17. Loria, J. P., Rance, M. & Palmer, A. G. A relaxation-compensated Carr–Purcell–Meiboom–Gill sequence for characterizing chemical exchange by NMR spectroscopy. *J. Am. Chem. Soc.* **121,** 2331–2332 (1999).
18. Tobler, K., Kelly, M. L., Pinto, L. H. & Lamb, R. A. Effect of cytoplasmic tail truncations on the activity of the M(2) ion channel of influenza A virus. *J. Virol.* **73,** 9695–9701 (1999).
19. Pinto, L. H. & Lamb, R. A. Understanding the mechanism of action of the anti-influenza virus drug amantadine. *Trends Microbiol.* **3,** 271 (1995).
20. Astrahan, P., Kass, I., Cooper, M. A. & Arkin, I. T. A novel method of resistance for influenza against a channel-blocking antiviral drug. *Proteins* **55,** 251–257 (2004).
21. Subczynski, W. K., Wojas, J., Pezeshk, V. & Pezeshk, A. Partitioning and localization of spin-labeled amantadine in lipid bilayers: an EPR Study. *J. Pharm. Sci.* **87,** 1249–1254 (1998).
22. Wang, J. F., Schnell, J. R. & Chou, J. J. Amantadine partition and localization in phospholipids membrane: a solution NMR study. *Biochem. Biophys. Res. Commun.* **324,** 212–217 (2004).
23. Griffin, S. D. *et al.* The p7 protein of hepatitis C virus forms an ion channel that is blocked by the antiviral drug, Amantadine. *FEBS Lett.* **535,** 34–38 (2003).
24. Plugge, B. *et al.* A potassium channel protein encoded by chlorella virus PBCV-1. *Science* **287,** 1641–1644 (2000).
25. Svensson, T. H. Dopamine release and direct dopamine receptor activation in the central nervous system by D-145, an amantadine derivative. *Eur. J. Pharmacol.* **23,** 232–238 (1973).

26. Swartz, K. J. & MacKinnon, R. Hanatoxin modifies the gating of a voltage-dependent K^+ channel through multiple binding sites. *Neuron* **18**, 665–673 (1997).
27. Lee, S.-Y. & MacKinnon, R. A membrane-access mechanism of ion channel inhibition by voltage sensor toxins from spider venom. *Nature* **430**, 232–235 (2004).
28. Stouffer, A. L. *et al.* Structural basis for the function and pharmaceutical inhibition of an influenza virus proton channel. *Nature* doi:10.1038/nature06528 (this issue).
29. Call, M. E. *et al.* The structure of the ζζ transmembrane dimer reveals features essential for its assembly with the T cell receptor. *Cell* **127**, 355–368 (2006).
30. Chou, J. J., Baber, J. L. & Bax, A. Characterization of phospholipids mixed micelles by translational diffusion. *J. Biomol. NMR* **29**, 299–308 (2004).
31. Oxenoid, K. & Chou, J. J. The structure of phospholamban pentamer reveals a channel-like architecture in membranes. *Proc. Natl Acad. Sci. USA* **102**, 10870–10875 (2005).

Supplementary Information is linked to the online version of the paper at www.nature.com/nature.

Acknowledgements We thank M. Berardi for many discussions, and S. Harrison for discussion and assisting with the manuscript. This work was supported by the NIH and the Pew Scholars Program in the Biomedical Sciences awarded to J.J.C. J.R.S. is supported by an NIH F32 postdoctoral fellowship.

Author Contributions J.R.S. and J.J.C. designed research, performed research, analysed data and wrote the paper.

Author Information The structures have been deposited in the Protein Data Bank under the accession number 2RLF. Reprints and permissions information is available at www.nature.com/reprints. The authors declare competing financial interests: details accompany full-text HTML version of the paper on www.nature.com/nature. Correspondence and requests for materials should be addressed to J.J.C. (james_chou@hms.harvard.edu).

METHODS

Sample preparation. M2(18–60) was expressed into inclusion bodies as a fusion to His_9–trpLE[32]. The M2(18–60) peptide was released from the fusion protein by cyanogen bromide digestion in 70% formic acid (2 h, 0.2 g ml^{-1}). The digest was dialyzed to water, lyophilized, and loaded onto a C4 column (Grace–Vydac) in 2:1:2 hexafluoroisopropanol:formic acid:water and separated on a gradient of 3:2 isopropanol:acetonitrile. The lyophilized peptide was refolded at 250 μM by dissolving in 6 M guanidine and 150 mM DHPC and dialyzing against the final NMR buffer containing 40 mM sodium phosphate and 30 mM glutamate. The sample was concentrated to a final M2(18–60) concentration of 0.75 mM (monomer). Rimantadine was added after concentrating. The concentration of DHPC was determined from ^{1}H NMR spectroscopy to be around 300 mM.

NMR spectroscopy. NMR experiments were conducted at 30 °C on spectrometers equipped with cryogenic probes (Bruker). Sequence-specific assignment of backbone ^1H_N, ^{15}N, ^{13}Cα and ^{13}Cβ chemical shifts were accomplished using the TROSY versions of the HNCA (^1H_N, ^{15}N and ^{13}Cα correlation spectroscopy) and HNCACB (^1H_N, ^{15}N and ^{13}Cβ correlation spectroscopy) experiments on a ^{15}N-, ^{13}C- and 85% ^{2}H-labelled protein. Side-chain χ_1 and χ_2 rotamers were obtained from measurements of the three-bond scalar couplings including $^3J_{NC\gamma}$, $^3J_{C'C\gamma}$ and $^3J_{C\alpha C\delta}$ (refs 33, 34) ^{1}H-^{15}N RDCs were measured for the protein–detergent complex weakly aligned in radially compressed polyacrylamide gel[35]. Intramonomer NOEs involving both backbone and side-chain protons were assigned using the three-dimensional ^{15}N-edited and ^{13}C-edited NOESYs recorded with NOE mixing times of 110 and 150 ms, respectively, on a sample containing ^{15}N-, ^{13}C-labelled protein, rimantadine, and deuterated DHPC (D35-DHPC; Avanti Polar Lipids, Inc.).

For identifying contacts between adjacent monomers, intramonomer NOEs were first assigned to completion. This is possible owing to the low complexity of the NOESY spectra of M2(18–60) (see Supplementary Figs 4 and 5). The remaining NOEs involving residues of the transmembrane and amphipathic helices, which could not be explained by intramonomer distances based on the known secondary structures, were identified to be intermonomer NOEs. The assignment of intermonomer distance restraints and structure calculation was carried out iteratively until all NOE cross peaks in the NOESY spectra were self-consistent in the tetrameric structure. Protein–drug NOEs were first identified using the ^{15}N-edited and ^{13}C-edited NOESYs described above, and subsequently confirmed by a ^{15}N-edited NOESY recorded with 500-ms mixing time on a sample containing uniform ^{15}N- and ^{2}H-labelled protein, rimantadine, and D35-DHPC.

Structure determination. Structures were calculated using the program XPLOR-NIH[36]. The secondary structure of the monomer was first calculated from its random coil using intramonomer NOEs, backbone dihedral restraints derived from chemical shifts (TALOS)[37] and side-chain χ_1 and χ_2 restraints shown in Supplementary Table 2. A total of 20 monomer structures were calculated using a standard high-temperature simulated annealing protocol in which the bath temperature was cooled from 1,000 K to 200 K. To obtain an initial set of tetramer structures, four copies of the lowest-energy monomer structure calculated above were used. The same high-temperature simulated annealing run was performed in the presence of intermonomer NOEs and all other intramonomer restraints except RDCs. For each experimental intermonomer NOE between two adjacent subunits, four identical distance restraints were assigned, respectively, to all pairs of neighbouring subunits to satisfy the condition of C4 rotational symmetry. During the annealing run, the bath was cooled from 1,000 K to 200 K with a temperature step of 20 K, and 6.7 ps of Verlet dynamics at each temperature step, using a time step of 3 fs. A total of 100 tetramer structures were calculated and independently cross-validated by ^{1}H-^{15}N RDCs.

Fitting of RDCs to structures was done by singular value decomposition using the program PALES[38]. The goodness of fit was assessed by Pearson correlation coefficient (r) and quality factor (Q). Among the 100 structural models, 15 structures in which the individual subunits have on average the best agreement with RDCs (r of ~0.91 and Q of ~0.25) were selected for a final, low-temperature refinement against RDCs in the presence of all NOE and dihedral restraints. During the refinement, the bath was cooled from 200 K to 20 K with a temperature step of 10 K, and 6.7 ps of Verlet dynamics at each temperature step, using a time step of 3 fs. The force constants for NOE and experimental dihedral restraints were fixed at 100 kcal mol^{-1} $Å^{-2}$ and 40 kcal mol^{-1} rad^{-2}, respectively. RDC restraint force constant was ramped from 0.01 to 0.125 kcal mol^{-1} Hz^{-2}. The force constant for RDCs was set to a small value to prevent violation of NOE restraints. For each of the 15 structures validated by RDCs, 10 RDC-refined structures were generated. From that set, the structure with the lowest total energy was added to the final ensemble to describe the structural diversity of the solution structure. The structure with heavy atom conformation closest to the mean was chosen to represent the final ensemble. Without violating any NOE restraints, the final subunit structures fit RDCs to r of 0.98 and Q of 0.15, with $D_a = 14.2$ Hz and $R_h = 0.24$. Final backbone r.m.s. deviation from the mean in the transmembrane and amphipathic domains were 0.30 Å and 0.56 Å, respectively.

Measurement of chemical exchange in the Trp 41 indole ring. The timescale of chemical shift exchange of the Trp 41 side chain was measured using a relaxation-compensated CPMG experiment[17] in 1D mode at ^{1}H frequency of 600 MHz. The dependence of ^{15}N relaxation owing to chemical exchange on the frequency of refocusing ($1/\tau_{cp}$) of chemical shift evolution was fitted to a two-site exchange model given by $R_{ex} \propto 1 - (2\tau_{ex}/\tau_{cp})\tanh(\tau_{cp}/2\tau_{ex})$, where R_{ex} is the contribution to transverse relaxation owing to chemical shift exchange, and τ_{ex} is the correlation time of the process that is generating the chemical shift exchange[39].

32. Blacklow, S. C. & Kim, P. S. Protein folding and calcium binding defects arising from familial hypercholesterolemia mutations of the LDL receptor. *Nature Struct. Biol.* **3,** 758–762 (1996).
33. Bax, A. *et al.* Measurement of homo- and heteronuclear J couplings from quantitative J correlation. *Methods Enzymol.* **239,** 79–105 (1994).
34. MacKenzie, K. R., Prestegard, J. H. & Engelman, D. M. Leucine side-chain rotamers in a glycophorin A transmembrane peptide as revealed by three-bond carbon-carbon couplings and 13C chemical shifts. *J. Biomol. NMR* **7,** 256–260 (1996).
35. Chou, J. J., Gaemers, S., Howder, B., Louis, J. M. & Bax, A. A simple apparatus for generating stretched polyacrylamide gels, yielding uniform alignment of proteins and detergent micelles. *J. Biomol. NMR* **21,** 377–382 (2001).
36. Schwieters, C. D., Kuszewski, J., Tjandra, N. & Clore, G. M. The Xplor-NIH NMR molecular structure determination package. *J. Magn. Reson.* **160,** 66–74 (2002).
37. Cornilescu, G., Delaglio, F. & Bax, A. Protein backbone angle restraints from searching a database for chemical shift and sequence homology. *J. Biomol. NMR* **13,** 289–302 (1999).
38. Zweckstetter, M. & Bax, A. Prediction of sterically induced alignment in a dilute liquid crystalline phase: aid to protein structure determination by NMR. *J. Am. Chem. Soc.* **122,** 3791–3792 (2000).
39. Allerhand, A. & Thiele, E. Analysis of Carr–Purcell spin-echo NMR experiments on multiple-spin systems. II. The effect of chemical exchange. *J. Chem. Phys.* **45,** 902–916 (1966).